NUCL SCI TECH (2021) 32:94
https://doi.org/10.1007/s41365-021-00932-9

Neutronic analysis of deuteron-driven spallation target

Wei-Wei Qiu[1] · Wu Sun[1] · Jun Su[1]

Received: 19 January 2021 / Revised: 15 June 2021 / Accepted: 16 July 2021 / Published online: 8 September 2021

Abstract Deuteron-driven spallation targets have garnered attention recently because they can provide high-energy neutrons to transmute long-lifetime fission products. In this study, the Geant4 toolkit was used to simulate the interaction between a deuteron beam at 500 MeV and a composite target composed of alternating lead-bismuth eutectic (LBE) and water. The water was used because it may be employed as a target coolant. The energy spectrum, neutron yield, average energy, and total energy of the emitted neutrons were calculated for different thicknesses and thickness ratios between the LBE and water. For a constant target thickness, the neutron yield increases with an increasing thickness ratio of LBE to H_2O, while the average energy of the emitted neutrons decreases with an increasing in the aforementioned thickness ratio . These two aspects support the use of a pure target, either LBE or water. However, with an increasing LBE-to-H_2O thickness ratio, the total energy of the emitted neutrons increases and then decreases. This result supports the addition of water into the LBE target. The angular distributions of the emitted neutrons show that the rear of the target is suitable for loading nuclear waste containing minor actinides and long-lifetime fission products.

Keywords Long-lived nuclear waste product · Accelerator-driven sub-critical system · Deuteron-induced spallation target · Neutron spectrum

1 Introduction

Nuclear energy is a clean energy source as it creates minimal pollution, releases only small amounts of greenhouse gases, and enables convenient transportation of fuels [1]. However, nuclear waste is an obstacle to the development of nuclear energy. For example, in China, if nuclear power plants are developed to have an installed capacity of approximately 100 million kilowatts by 2030, more than 20,000 tons of nuclear waste will be produced [2]. Twenty tons of them are long-lived minor actinides (MA). Thus far, burial deep in the ground has been a relatively safe disposal method for nuclear waste [3]. However, because nuclear waste must be stored for hundreds or even millions of years before its radioactivity becomes sufficiently low, the public are still skeptical about the deep burying [4–6].

Another possible method to deal with nuclear waste is transmutation. Since the early 1990s, with the development of large currents and high-power accelerators, a new nuclear waste treatment method, i.e., transmutation based on an accelerator-driven subcritical system (ADS), has been proposed and widely studied [7–9]. ADS consists of an accelerator, spallation target, and subcritical system [10]. The accelerator provides a stream of particles to bombard the spallation target, thereby producing hard neutrons. Then, hard neutrons induce nuclear reactions with long-lived nuclei in a subcritical system [10]. Therefore, ADS is a good choice for transmuting MA [11–13].

This work was supported by the National Natural Science Foundation of China (No. 11875328).

✉ Jun Su
sujun3@mail.sysu.edu.cn

[1] Sino-French Institute of Nuclear Engineering and Technology, Sun Yat-sen University, Zhuhai 519082, China

When the products of long-lived nuclei are less than those of short-lived or stable nuclei, the radioactivity is sufficiently low [14]. It has been reported that the storage time of nuclear waste after transmutation can be reduced from 100,000 to 300 years [7]. Simultaneously, ADS generates thermal energy that can be used for power generation. For example, the ADS project of the Japan Atomic Energy Agency will produce 800 MW, which is similar to that of a general nuclear power unit [15]. Approximately 10% of the generated electrical energy is used to drive the accelerator to emit a particle beam [7]. In addition, in a well-designed ADS system, the subcritical reactor immediately stops the reaction after cutting off the supply of the neutron source [16].

Since 1990, the European Union, the USA, Japan, and other countries and regions have carried out research on ADS projects [16–18]. China started ADS concept research in the 1990s. In 2011, the Chinese Academy of Sciences implemented a strategic pilot technology project "Future Advanced Nuclear Fission Energy". The ADS transmutation system is one of the two major parts of this project. The purpose is to establish an ADS demonstration system that can be industrially promoted. To achieve this goal, the development of an ADS transmutation system includes three phases. In phase 1, the key technical problems of the ADS will be solved, including the establishment of discrete small systems such as accelerators, spallation targets, subcritical reactors, and experience in debugging the ADS. In phase 2, technical verification will be conducted to establish an ADS experimental device with a 500-MeV driven linac [19]. In phase 3, an exemplary ADS device will be built, and the ADS will be commercialized on a large scale [2]. At present, China is still in phase 1. At this phase, Chinese researchers have conducted many related studies on ADS, and some nuclear data measurement facilities have been developed [8]. In addition, the preparation of high-energy neutron cross section libraries and the simulation of ADS spallation target neutrons through the Monte Carlo codes FLUKA, MCNPX, and OpenMC have also attracted wide attention [20–23].

As one of the three major parts of ADS, the design and optimization of spallation targets have also received much attention. Diverse designs for spallation targets regarding shape and material have been proposed [24, 25]. In the experimental demonstration of the technological feasibility of transmutation in an accelerator-driven system (XT-ADS), the multi-purpose Hybrid Research Reactor for High-tech Applications (MYRRHA), and the Japan Atomic Energy Agency-Accelerator-Driven System (JAEA-ADS), a lead-bismuth eutectic (LBE) rod target at the center of the reaction core was used [26]. XT-ADS and MYRRHA use windowless targets [27], whereas JAEA-ADS uses targets with proton windows [18]. For the China Initiative Accelerator-Driven System program (Ci-ADS), researchers have conducted research on LBE rod targets [28], but others have proposed innovative spallation targets. For example, Yang Lei and Zhan Wenlong proposed a new spallation target concept involving a gravity-driven dense granular target (DGT) [29]. This target is similar to an hourglass and has the advantages of both solids and fluids. However, reducing the wear of particles is also a challenge. Although the DGT is still imperfect, it has also led many researchers to conduct various research projects, including neutron research and energy deposition on the DGT [30, 31].

Regarding target materials, LBE, lead, or tungsten is commonly used in ADS designs [2]. The spallation target influences the energy spectrum of the neutron source in the ADS. Because of the widespread use of proton beams in ADS internationally, many researchers have conducted systematic neutron studies, including parameters such as neutron yield, energy spectrum, and angle distribution, based on the impact of proton beams on various spallation targets, with which the optimal design of the spallation target is proposed [32].

Because thermal neutrons cannot effectively transform long-lived fission products, the high-energy neutron yield is particularly important in spallation target design. Proton-driven targets are currently widely used in various ADS devices. However, many researchers still focus on deuteron-driven spallation targets. Krasa et al. studied the effect of deuterons and protons on the neutron yield, and Adam et al. experimentally measured the reaction rates of various isotopes with deuteron spallation reactions [33, 34]. Compared with proton-driven spallation targets, deuteron-driven spallation targets can generate more high-energy neutrons. This paper focuses on a spallation target driven by a deuteron beam. The study is organized as follows. In Sect. 2, the model is described. In Sect. 3, both the results and discussion are presented. Finally, a summary is provided in Sect. 4.

2 Tools and model

In this work, the Geant4 toolkit was used to simulate the interaction between the deuteron beam and target. Geant4 is a Monte Carlo application toolkit developed by CERN, based on the C++ language. It is used to simulate the physical process of particle transport in matter. It is widely used in high-energy physics research, accelerator construction, and medical fields. It is also used for simulating spallation targets. Geant4 has been used to calculate the energy deposition [35, 36] and to obtain outgoing neutron data [37]. In this study, Geant4 version 10.5 (patch-01, released April 17, 2019) was used with the databases

G4NDL4.6 and G4TENDL1.3.2, which are from TENDL-2014 [38], the ENDF/B-VII library [39], and the JENDL library in the Ubuntu 18.04 system.

The spallation target is a flat cylindrical shape with a radius of 22 cm. Its thickness varies from 1 to 50 mm. The spallation target material is LBE. LBE contains 45% lead and 55% bismuth, with a density of approximately 10.68 g/cm^3. The water is located between two flat cylindrical shapes. The entire target (LBE + water) is in a vacuum. The specific model of the target is shown in Fig. 1.

A hollow sphere with a radius of 70 cm was used as the detector, so that neutrons could be detected in all directions. The hollow spherical detector was wrapped with a composite target consisting of six layers of flat cylindrical targets and water between the targets. A 10 cm × 10 cm square deuteron beam at 500 MeV was coaxial with the target and incident from the direction (0,0,1) in the simulation.

3 Results and discussion

3.1 Pure H_2O and LBE targets

The first step of the simulation was to determine the thickness of the composite target. Pure H_2O and LBE targets are considered . The number of deuterons emitted as a function of the target thickness is shown in Fig. 2. The number of outgoing deuterons first decreases exponentially as a function of the target thickness and then decreases rapidly to zero. The exponential damping is caused by the nuclear reaction, whereas the range is determined by the stopping power. As shown in Fig. 2, the range of deuterons at 500 MeV in H_2O is 740 mm, and that in LBE is 140 mm. In the following, the thickness of the spallation target is chosen according to these ranges.

Figure 3 shows the energy spectra of the emitted neutrons from a 140-mm pure LBE target, 140-mm pure H_2O target, and 740-mm pure H_2O target.

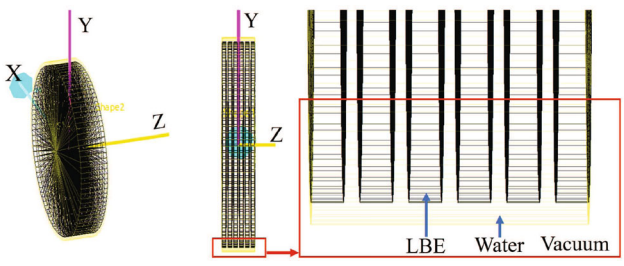

Fig. 1 (Color online) Composite target structure diagram; 6 LBE target and 5 interstitial water layers are used

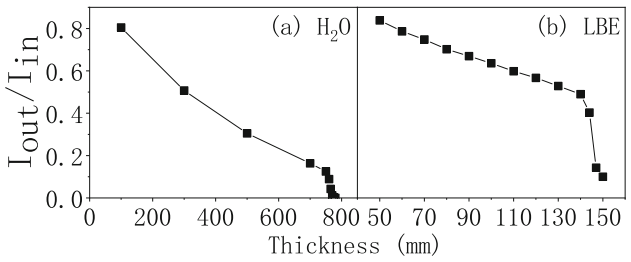

Fig. 2 Number of emitted deuterons as a function of target thickness for pure H_2O and LBE

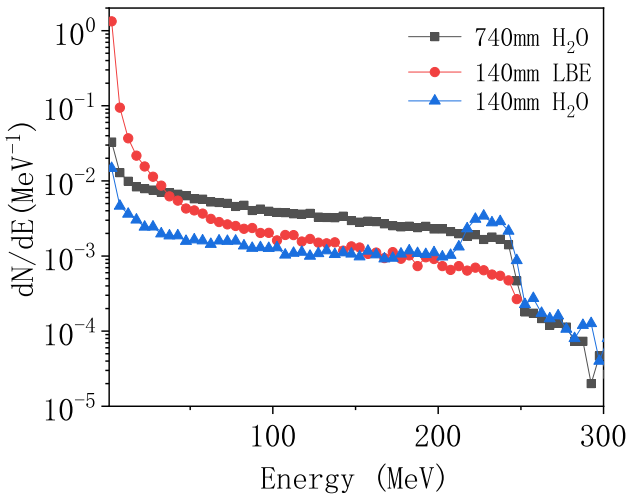

Fig. 3 (Color online) Energy spectra of emitted neutron from 140-mm pure LBE target, 140-mm pure H_2O target, and 740-mm pure H_2O target

For the 140-mm H_2O target, the energy spectrum exhibited a peak at 250 MeV. The neutrons at 250 MeV are produced from proton stripping of the deuteron. When using the 740-mm H_2O target, the peak disappears, and the neutron yield decreases monotonically with energy. In other words, thermal neutrons dominate. In fact, after the neutrons are produced in the nuclear reaction of deuterons with H and O, they pass through the target a few hundred millimeters before exiting. Thermal neutrons are not only directly derived from nuclear reactions, but also from the slowing down of neutrons. This indicates that water has two roles with respect to the outgoing neutrons, i.e., production of high-energy neutrons and slowing down of the neutrons.

Comparing the energy spectra for the LBE and H_2O targets with the same thickness (140 mm), we find different roles for LBE and H_2O. For energies less than 100 MeV, the neutron yield from the LBE target is larger than that from the H_2O target. However, in the region near 250 MeV, the neutrons from the H_2O target are more abundant. This indicates that proton stripping occurs in the H_2O target, but spallation dominates in the LBE target. The

former results in high-energy neutrons, whereas the latter causes fast and slow neutrons.

Furthermore, the amount of thermal and slow neutrons from the LBE target is much higher than that from H_2O. This is one of the reasons why heavy metal targets are commonly used in spallation targets. However, water is helpful for increasing the energy of the outgoing neutrons from the spallation target. Heat dissipation from the pure metal target is poor, and water flow is also helpful for dissipating heat.

3.2 Yield, average energy, and total energy of neutrons from composite target

Six LBE slices were used, with H_2O filling in each interval. The total thickness of the composite target in the simulation was 140, 240, 340, 440, 540, 640, or 740 mm.

The energy spectra for the 140-mm spallation target are shown in Fig. 4a. The neutron energy spectra for spallation targets with various LBE-to-H_2O thickness ratios show the characteristic of decreasing with energy. In other words, for all LBE-to-H_2O thickness ratios of spallation targets, thermal neutrons are the most emitted neutrons. In addition, there is a gentler platform at approximately 1 MeV. This shows that the water has a significant slowing effect on neutrons. A large number of hard neutrons produced by the nuclear reaction of the deuteron become thermal neutrons after elastic collisions.

It is clear that targets with a sufficiently low LBE-to-H_2O thickness ratio are not suitable for spallation targets. In addition, the neutron energy spectrum also shows a decreasing trend in the high-energy region with decreasing LBE-to-H_2O thickness ratio. The platforms around 1 MeV also gradually disappear when the LBE-to-H_2O thickness ratio decreases. This is due to the continuous thickening of the water layer. The slowing down of outgoing neutrons by water becomes increasingly obvious.

As shown in Fig. 4, all neutron spectra of the composite target with thicknesses ranging from 240 to 740 mm show a similar trend. In other words, the neutron energy spectra for various LBE-to-H_2O thickness ratios show the characteristic of decreasing with energy. At approximately 1 MeV, the spectra have a relatively gentle platform. In addition, the neutron energy spectra also show a decreasing trend in the high-energy region as the LBE-to-H_2O thickness ratio decreases, and the platforms at approximately 1 MeV also gradually disappear. In addition, it can be found that under the same LBE thickness target, the energy spectra with thick water are relatively similar. For example, the energy spectra of the 440-mm spallation target were more dispersed, while the energy spectra of the 740-mm spallation target were denser. This is due to the slowing down effect of the neutron caused by water. The slowing down effect with thicker water is more obvious.

The neutron yield, average energy, and total energy were analyzed further.

Figure 5 shows the neutron yield as a function of the LBE-to-H_2O thickness ratio d(LBE):d(H_2O). As the LBE-to-H_2O thickness ratio increases, so does the neutron yield. The outgoing neutrons mostly originate from the collision process between the deuteron and the LBE target. The spallation cross section of deuteron in water is smaller than that in LBE. Therefore, for a constant total thickness, more neutrons will be emitted with a thicker LBE target. In the low LBE-to-H_2O thickness ratio and low thickness regions, for the same LBE-to-H_2O thickness ratio, the neutron yield also increases with increasing total thickness. This phenomenon is consistent with the previous analysis. However, for large LBE-to-H_2O thickness ratios [d(LBE):d(H_2O) > 0.8] or large thicknesses (thickness $>$ 540 mm), the neutron yield is very similar.

First, in the large LBE-to-H_2O thickness ratio region, with a thicker LBE, the neutron yield is higher. However, thick water also has a suppressive effect on the production of neutrons. The water could slow down the deuteron and

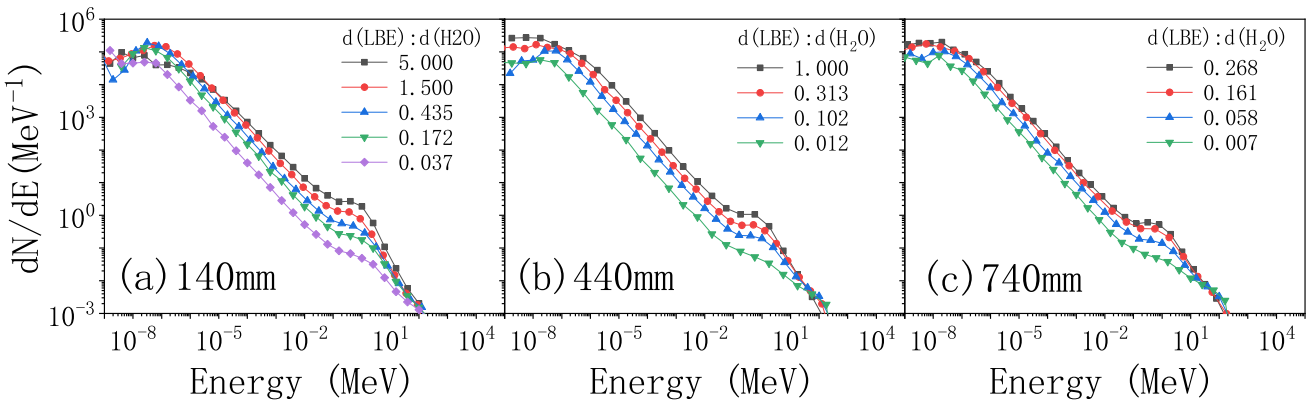

Fig. 4 (Color online) Neutron spectra (normalized to 1 incident deuteron) of the composite target with thickness ranging from 240 to 740 mm

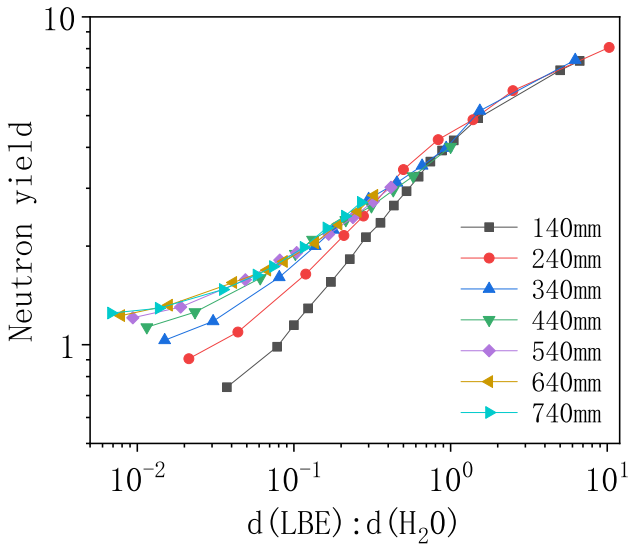

Fig. 5 (Color online) Neutron yield (normalized to 1 incident deuteron) as a function of LBE-to-H_2O thickness ratio

hence reduce the cross section of the deuteron and LBE. These effects maintain the balance between the neutron yield and the thickness of the target. Second, in the large thickness region, the phenomenon is similar when the LBE-to-H_2O thickness ratio is larger than 0.1. However, for d(LBE):d(H_2O) < 0.1, with a larger total thickness, neutron yield is higher. Because the thickness of the LBE is much smaller than that of H_2O, the deuterons mostly react with water.

High-energy neutron (>1 MeV) yields were also counted, as shown in Fig. 6, where it can be seen that the overall trend in Fig. 6 is essentially the same as in Fig. 5. To transmute MA (e.g., 241 Am, with an effective neutron energy for transmutation higher than 1 MeV), either Fig. 5 or 6 can be used with little effect on the results.

The pure LBE targets for all thicknesses resulted in the largest neutron yields compared with the composite target. With the goal to produce more neutrons, it is a good choice to use pure LBE as the target material. This advantage of the LBE target will be weakened if water is added as a coolant.

Figure 7 shows the average energy of neutrons with various total thicknesses and LBE-to-H_2O thickness ratios. Comparing the calculations for the same total thickness, the average energy of outgoing neutrons decreases with increasing LBE-to-H_2O thickness ratio. It was found in the above subsection that the energy spectrum for H_2O is harder than that for the LBE. With the same total thickness, the increase in the LBE-to-H_2O thickness ratio indicates an increase in LBE thickness, which results in more thermal neutrons and hence a lower average energy of the neutron. Comparing the calculations for the same LBE-to-H_2O thickness ratio, the average energy of the emitted neutrons decreases with increasing total thickness. This trend is more obvious for small LBE-to-H_2O thickness ratios. When the LBE-to-H_2O thickness ratio is the same, an increase in the total thickness means more LBE and water. Stopping the incident deuteron and moderation of the neutron both decrease the average energy. The analysis of the average neutron energy indicates that the water, rather than the LBE target, should be applied to increase the energy of outgoing neutrons.

The analysis of the neutron yield and average energy supports different target materials. It is suggested to balance this contradiction using the total energy of neutrons.

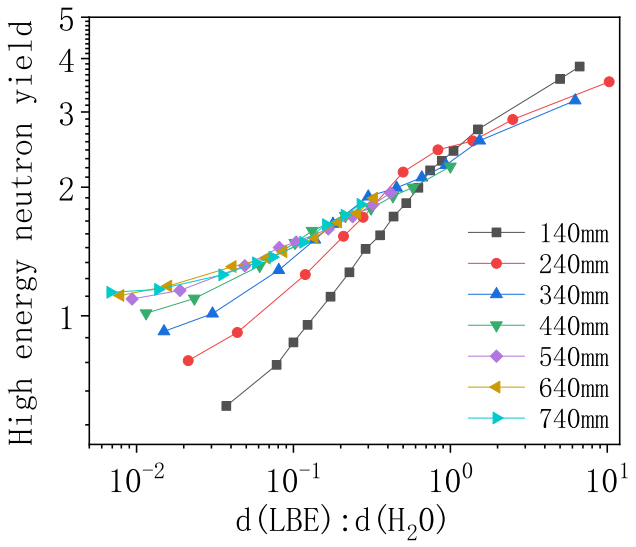

Fig. 6 (Color online) High-energy neutron(>1 MeV) yield (normalized to 1 incident deuteron) as a function of LBE-to-H_2O thickness ratio

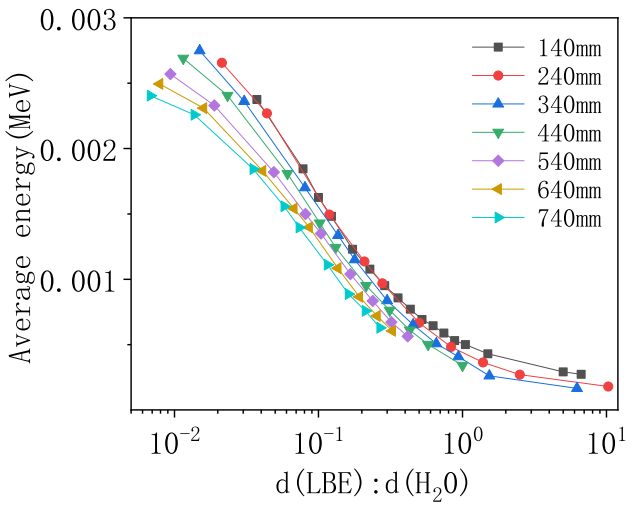

Fig. 7 (Color online) Average energy of emitted neutrons as a function of LBE-to-H_2O thickness ratio

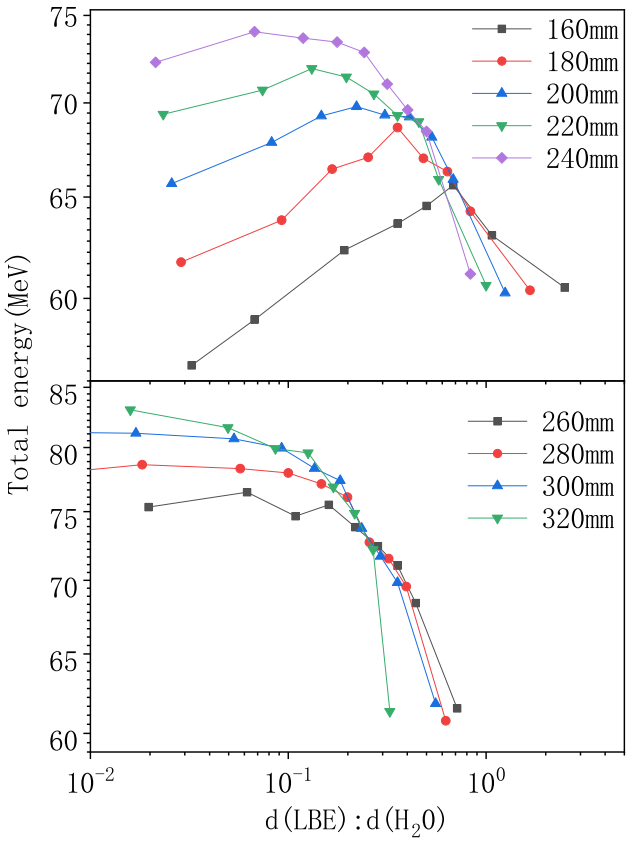

Fig. 8 (Color online) Total energy of emitted neutrons (normalized by 1 incident deuteron) as a function of LBE-to-H_2O thickness ratio

Figure 8 shows the total energy of the emitted neutrons (normalized by 1 incident deuteron) as a function of the LBE-to-H_2O thickness ratio. For a thin target (160–240 mm), the total energy:not_found increases and then decreases with increasing LBE-to-H_2O thickness ratio. This is the result of competition between the increasing neutron yield and decreasing average neutron energy. We call the LBE-to-H_2O thickness ratio with the highest total energy the optimal ratio. However, for a thick target (260–320 mm), the total energy decreases with increasing LBE-to-H_2O thickness ratio. Figure 8 shows the trend of the LBE-to-H_2O thickness ratio of the total neutron energy emitted by 160–320 mm spallation targets. Before the saturation of LBE, the total energy increases with the thickness of the spallation target. After reaching saturation, when viewed together with Fig. 9, the total energy decreases as the spallation target thickness increases. The optimal ratio also appears in the spallation target of 160–280 mm, and as the thickness increases, the LBE-to-H_2O thickness ratio gradually decreases. The optimal ratio disappears when the spallation target thickness is greater than 300 mm. For thicker targets, the water layer is thicker, which affects the saturation thickness of the LBE.

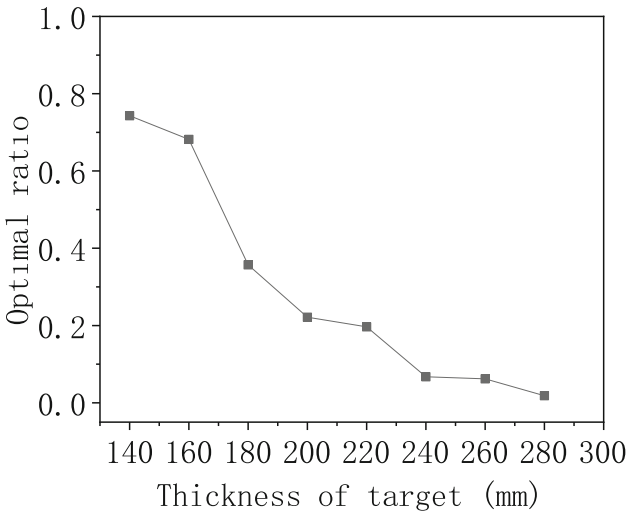

Fig. 9 The optimal ratio as a function of composite target thickness for 30,000 incident deuterons at 500 MeV

Obviously, with a thicker water layer, the saturation thickness of the LBE is smaller.

3.3 Angular distribution of neutrons

The angular distribution of the average energy of the emitted neutrons is shown in Fig. 10. The average energy of the emitted neutrons increases along the direction of deuteron incidence, with a minimum at 180° and a maximum at 0°. The angular distribution of neutrons from a deuteron-induced target is not fundamentally different from that from a proton-induced target.

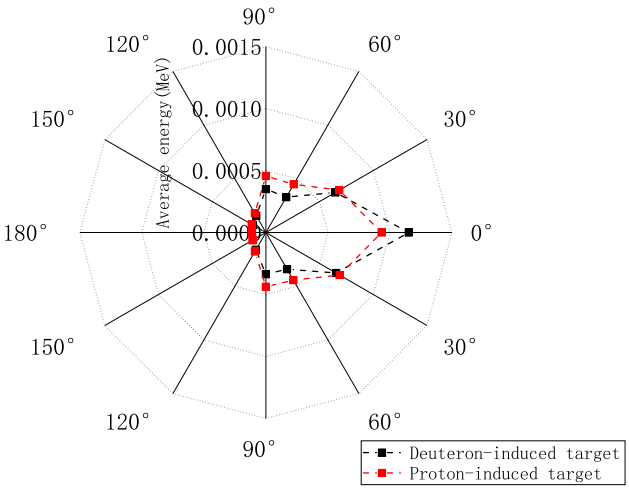

Fig. 10 (Color online) Angular distribution of the average energy of emitted neutrons (normalized by 1 incident deuteron/proton). 500-MeV deuterons are incident on the 85-mm composite target from the (0,0,1) direction in the 0°–180° axis. The composite target was placed at the origin

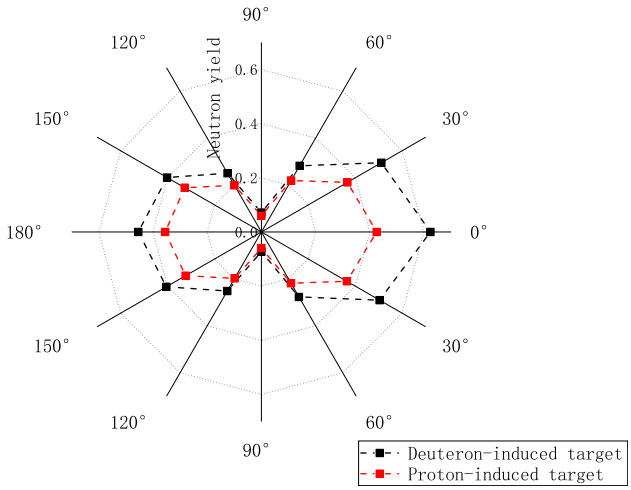

Fig. 11 (Color online) Angular distribution of the neutron yield (normalized by 1 incident deuteron/proton). 500-MeV deuterons are incident on the 85-mm composite target from the (0,0,1) direction in the 0°–180° axis. The composite target was placed at the origin

However, as shown in Fig. 11, the neutron yield of a deuteron-induced target is higher than that of a proton-induced target in all directions, especially in the 0° direction.

The angular distribution of the total energy of the emitted neutrons is shown in Fig. 12. The total neutron energy is distributed evenly in front of the target, with minimum and maximum values at 90° and 0°, respectively. The total neutron energy from the deuteron-induced target was significantly higher than that from a proton-induced target in the 0° direction.

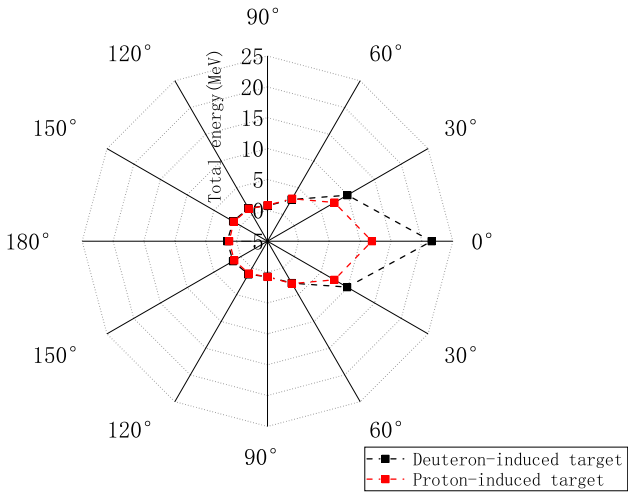

Fig. 12 (Color online) Angular distribution of the total energy of emitted neutrons (normalized by 1 incident deuteron/proton). 500-MeV deuterons are incident on the 85-mm composite target from the (0,0,1) direction in the 0°–180° axis. The composite target was placed at the origin

Through analysis of the angular distribution, it was found that the angular distribution of neutrons produced by a deuteron-induced target shows results similar to those of a proton-induced target. That is, the neutron yield, average energy, and total energy in front of the target are significantly smaller than those at the back of the target. Thus, when filling in spent fuel, more spent fuel is filled behind the target.

In addition, in the forward direction, we found that the neutron yield and total neutron energy of the deuteron-induced target were significantly higher than those of a proton-induced target. This occurs because, when the break-up reaction of the deuteron dominates, and after proton stripping, there are more secondary neutrons that still follow the original trajectory and eventually exit. This phenomenon indicates that deuteron-induced targets produce more high-energy neutrons than proton-induced targets in the forward direction.

4 Conclusion

Proton-driven spallation targets are commonly used in accelerator-driven subcritical systems (ADSs). Recently, deuteron-driven spallation targets have received attention because they can provide high-energy neutrons.

In this study, we performed a neutronic analysis of a deuteron-induced spallation target. The cylindrical composite LBE to H_2O target was established using the Geant4 toolkit. Then, the energy spectrum, yield, average energy, total energy, and angular distribution of the emitted neutrons from the interaction between the deuteron beam and the cylindrical LBE to H_2O composite target were studied. The thickness and LBE-to-H_2O thickness ratio of the target were changed to optimize the emitted neutrons.

The neutron energy spectrum shows a decreasing trend in the high-energy region with decreasing LBE-to-H_2O thickness ratio. In other words, a pure LBE target produces the most high-energy neutrons. The energies of the neutrons produced in the spallation target decrease if water is added as a coolant.

The neutron yield increases with increasing LBE-to-H_2O thickness ratio. Hence, pure LBE targets of all thicknesses have the largest neutron yields. However, through analysis of the average neutron energy, it was found that with a larger LBE-to-H_2O thickness ratio, the average energy of the emitted neutrons decreased. Hence, neutrons emitted from the pure LBE target have the lowest average energy. By analyzing the total neutron energy, it was found that at a certain thickness, a specific LBE-to-H_2O thickness ratio has the highest total neutron energy. This LBE-to-H_2O thickness ratio is called the optimal ratio. The optimal ratio decreases with increasing thickness

and returns to zero (i.e., pure water) for a thickness of 340 mm. In other words, the total neutron energy is highest for pure water when the thickness of the spallation target is greater than 340 mm.

By analyzing the angular distribution, it was found that neutrons emitted along the direction of the deuteron beam had a higher neutron yield, average energy, and total energy. Therefore, neutrons emitted along the direction of the deuteron beam are more suitable for transmutation reactions. Hence, more nuclear waste can be placed behind the spallation target . In addition, the angular distribution shows that a deuteron-induced target produces more high-energy neutrons than a proton-induced target in the forward direction.

Author Contributions All authors contributed to the study conception and design. Material preparation, data collection, and analysis were performed by Wei-Wei Qiu, Wu Sun, and Jun Su. The first draft of the manuscript was written by Wei-Wei Qiu, and all authors commented on previous versions of the manuscript. All authors read and approved the final manuscript.

References

1. J.D. MacDonald, Safe and secure—environmental effects of nuclear power plants and the nuclear fuel cycle. IEEE Power Energy Mag. **4**, 49–55 (2006). https://doi.org/10.1109/PAE-M.2006.247870
2. W.L. Zhan, H.S. Xu, Advanced fission energy program-ads transmutation system. Bull. Chin. Acad. Sci. **27**, 375–381 (2012). https://doi.org/10.3969/j.issn.1000-3045.2012.03.017
3. B. Grambow, C. Landesman, S. Ribet, Nuclear waste disposal: I. Laboratory simulation of repository properties. Appl. Geochem. **49**, 237–246 (2014). https://doi.org/10.1016/j.apgeochem.2014.05.017
4. H. Kunreuther, D. Easterling, W. Desvousges et al., Public attitudes toward siting a high-level nuclear waste repository in nevada. Risk Anal. **10**, 469–484 (1990). https://doi.org/10.1111/j.1539-6924.1990.tb00533.x
5. C. McCombie, Nuclear waste management worldwide. Phys. Today **50**, 56–62 (1997). https://doi.org/10.1063/1.881779
6. C. Fairhurst, Nuclear waste disposal and rock mechanics: contributions of the underground research laboratory (URL), pinawa, manitoba, canada. Int. J. Rock Mech. Min. Sci. **41**, 1221–1227 (2004). https://doi.org/10.1016/j.ijrmms.2004.09.001
7. F. Venneri, M.A. Williamson, N. Li et al., Disposition of nuclear waste using subcritical accelerator-driven systems: technology choices and implementation scenarios. Nucl. Technol. **132**, 15–29 (2000). https://doi.org/10.13182/nt00-a3126
8. Z.Q. Chen, Recent progress in nuclear data measurement for ADS at IMP. Nucl. Sci. Tech. **28**, 184 (2017). https://doi.org/10.1007/s41365-017-0335-3
9. P. Yang, Z.K. Lin, W.S. Wan et al., Preliminary neutron study of a thorium-based molten salt energy amplifier. Nucl. Sci. Tech. **31**, 41 (2020). https://doi.org/10.1007/s41365-020-0750-8
10. H. Abderrahim, P. Kupschus, E. Malambu et al., MYRRHA: a multipurpose accelerator driven system for research & development. Nucl. Instrum. Methods Phys. Res. Sect. A **463**, 487–494 (2001). https://doi.org/10.1016/s0168-9002(01)00164-4
11. H. Nifenecker, S. David, J. Loiseaux et al., Basics of accelerator driven subcritical reactors. Nucl. Instrum. Methods Phys. Res. Sect. A **463**, 428–467 (2001). https://doi.org/10.1016/S0168-9002(01)00160-7
12. K. Tsujimoto, T. Sasa, K. Nishihara et al., Neutronics design for lead-bismuth cooled accelerator-driven system for transmutation of minor actinide. J. Nucl. Sci. Technol. **41**, 21–36 (2004). https://doi.org/10.1080/18811248.2004.9715454
13. H.Y. Meng, Y.W. Yang, Z.L. Zhao et al., Physical studies of minor actinide transmutation in the accelerator-driven subcritical system. Nucl. Sci. Tech. **30**, 91 (2019). https://doi.org/10.1007/s41365-019-0623-1
14. C.D. Bowman, Accelerator-driven systems for nuclear waste transmutation. Annu. Rev. Nucl. Part. Sci. **48**, 505–556 (1998). https://doi.org/10.1146/annurev.nucl.48.1.505
15. K. Tsujimoto, H. Oigawa, N. Ouchi et al., Research and development program on accelerator driven subcritical system in JAEA. J. Nucl. Sci. Technol. **44**, 483–490 (2007). https://doi.org/10.1080/18811248.2007.9711312
16. D.E. Beller, Overview of the AFCI reactor-accelerator coupling experiments (race) project. Trans.-Am. Nucl. Soc. **90**, 333–334 (2004)
17. D.D. Bruyn, H.A. Abderrahim, P. Baeten et al., The MYRRHA ADS project in Belgium enters the front end engineering phase. Phys. Proc. **66**, 75–84 (2015). https://doi.org/10.1016/j.phpro.2015.05.012
18. T. Sasa, H. Oigawa, K. Tsujimoto et al., Research and development on accelerator-driven transmutation system at JAERI. Nucl. Eng. Des. **230**, 209–222 (2004). https://doi.org/10.1016/j.nucengdes.2003.11.033
19. Z. Wang, Y. He, G. Huang, et al., in *10th International Particle Accelerator Conference*, The status of ciads superconducting linac. JACOW Publishing, Geneva, Switzerland, 2019. https://doi.org/10.18429/JACoW-IPAC2019-MOPTS059
20. Z.L. Zhao, Y.W. Yang, H.Y. Meng et al., Preparation and verification of mixed high-energy neutron cross-section library for ADS. Nucl. Sci. Tech. **29**, 140 (2018). https://doi.org/10.1007/s41365-018-0487-9
21. Z.Q. Liu, Z.L. Zhao, Y.W. Yang et al., Development and validation of depletion code system IMPC-burnup for ADS. Nucl. Sci. Tech. **30**, 44 (2019). https://doi.org/10.1007/s41365-019-0560-z
22. A.A.A. Qaaod, V. Gulik, 226ra irradiation to produce 225ac and 213bi in an accelerator-driven system reactor. Nucl. Sci. Tech. **31**, 44 (2020). https://doi.org/10.1007/s41365-020-00753-2
23. Z.L. Zhao, Y.W. Yang, S. Hong, Application of FLUKA and OpenMC in coupled physics calculation of target and subcritical reactor for ADS. Nucl. Sci. Tech. **30**, 10 (2019). https://doi.org/10.1007/s41365-018-0539-1
24. G. Bauer, Overview on spallation target design concepts and related materials issues. J. Nucl. Mater. **398**, 19–27 (2010). https://doi.org/10.1016/j.jnucmat.2009.10.005
25. F. Heidet, N.R. Brown, M.H. Tahar, Accelerator–reactor coupling for energy production in advanced nuclear fuel cycles. Rev. Accel. Sci. Technol. **08**, 99–114 (2015). https://doi.org/10.1142/s1793626815300066
26. A. Class, D. Angeli, A. Batta et al., XT-ADS windowless spallation target thermohydraulic design & experimental setup. J. Nucl. Mater. **415**, 378–384 (2011). https://doi.org/10.1016/j.jnucmat.2011.04.050
27. H.A. Abderrahim, P. D'Hondt, MYRRHA: A European experimental ADS for R & D applications status at mid-2005 and prospective towards implementation. J. Nucl. Sci. Technol. **44**, 491–498 (2007). https://doi.org/10.1080/18811248.2007.9711313
28. K. Chen, Y. Yang, D. Fan et al., Thermal hydraulic studies of lead–bismuth eutectic spallation target of CIADS. Nucl. Eng.

Des. **305**, 672–677 (2016). https://doi.org/10.1016/j.nucengdes.2016.06.025
29. L. Yang, W. Zhan, New concept for ADS spallation target: gravity-driven dense granular flow target. Sci. China Technol. Sci. **58**, 1705–1711 (2015). https://doi.org/10.1007/s11431-015-5894-0
30. Q. Zhao, W. Cui, Z. He et al., Energy deposition and neutron flux study in a gravity-driven dense granular target (DGT) with GEANT4 toolkit. Nucl. Instrum. Methods Phys. Res. Sect. B **427**, 63–69 (2018). https://doi.org/10.1016/j.nimb.2018.04.045
31. Q. Zhao, X.Y. Zhang, W.J. Cui et al., Numerical study on the inner temperature measurement for the target in CiADS. Nucl. Instrum. Methods Phys. Res. Sect. B **432**, 37–41 (2018). https://doi.org/10.1016/j.nimb.2018.07.017
32. Y.L. Zhang, X.C. Zhang, J. Qi et al., Study on the parameters of the ADS spallation target. J. Phys. Conf. Ser. **420**, 012064 (2013). https://doi.org/10.1088/1742-6596/420/1/012064
33. A. Krasa, V. Wagner, M. Majerle et al., Neutron production in a pb/u-setup irradiated with 0.7–2.5 gev protons and deuterons. Nucl. Instrum. Methods Phys. Res. Sect. A. Detect. Assoc. Equip. **615**, 70–77 (2010). https://doi.org/10.1016/j.nima.2010.01.029
34. J. Adam, V. Chilap, V. Furman et al., Study of secondary neutron interactions with 232th, 129i, and 127i nuclei with the uranium assembly "quinta"at 2, 4, and 8 gev deuteron beams of the jinr nuclotron accelerator. Appl. Radiat. Isot. **107**, 225–233 (2016). https://doi.org/10.1016/j.apradiso.2015.11.002
35. Y. Malyshkin, I. Pshenichnov, I. Mishustin et al., Neutron production and energy deposition in fissile spallation targets studied with geant4 toolkit. Nucl. Instrum. Methods Phys. Res. Sect. B **289**, 79–90 (2012). https://doi.org/10.1016/j.nimb.2012.07.023
36. A. Lamrabet, A. Maghnouj, J. Tajmouati et al., Assessment of the power deposition on the megapie spallation target using the geant4 toolkit. Nucl. Sci. Tech. **30**, 54 (2019). https://doi.org/10.1007/s41365-019-0590-6
37. S. Lee, C. Bungau, R. Cywinski, in *7th International Particle Accelerator Conference IPAC2016*, Geant4 simulations of proton-induced spallation for applications in ADSR systems (2016) https://doi.org/10.1007/s41365-019-0590-6
38. A. Koning, D. Rochman, Modern nuclear data evaluation with the talys code system. Nucl. Data Sheets **113**, 2841–2934 (2012). https://doi.org/10.1016/j.nds.2012.11.002
39. M. Chadwick, M. Herman, P. Obložinský et al., Endf/b-vii.1 nuclear data for science and technology: cross sections, covariances, fission product yields and decay data. Nucl. Data Sheets **112**, 2887–2996 (2011). https://doi.org/10.1016/j.nds.2011.11.002